

# Coherent quantum transport of charge density waves

J. H. Miller, Jr.\* and A. I. Wijesinghe†

*Department of Physics, University of Houston, Houston, Texas 77204-5005 USA and  
Texas Center for Superconductivity, University of Houston, Houston, Texas 77204-5002 USA*

Z. Tang

*Department of Chemistry, University of Houston, Houston, Texas 77204-5003 USA*

A. M. Guloy

*Texas Center for Superconductivity, University of Houston, Houston, Texas 77204-5002 USA and  
Department of Chemistry, University of Houston, Houston, Texas 77204-5003 USA*

(Dated: November 25, 2024)

Recent experiments show oscillations of period  $h/2e$  in conductance vs. magnetic flux of charge density wave (CDW) rings above 77 K, thus revealing macroscopically observable quantum behavior. The time-correlated soliton tunneling model discussed here is based on coherent, Josephson-like tunneling of microscopic quantum solitons of charge  $2e$ . The model interprets the CDW threshold electric field as a Coulomb blockade threshold for soliton pair creation and draws upon the theory of time-correlated single-electron tunneling to interpret CDW dynamics above threshold. As in Feynman's derivation of the Josephson effect, the picture treats the Schrödinger equation as an emergent 'classical' equation to describe the time-evolution of Josephson-coupled fluidic complex order parameters. Coupling of vector or time-varying scalar potentials to the order parameter phases enables  $h/2e$  quantum interference in CDW rings and also leads to interesting behavior of CDWs in response to oscillatory electric fields. The ability to vary both magnitudes and phases of the Josephson-coupled order parameters is crucial to any future applications in quantum computing.

## I. INTRODUCTION

Recent developments necessitate a transformation in our understanding of charge density wave (CDW) transport to one based on quantum principles.<sup>1</sup> The CDW is a correlated electron (or electron-phonon) system that, like a superconductor, can transport electrons through a quasi-one-dimensional or layered crystal *en masse*.<sup>2</sup> It is the only known such system capable, in the linear chain compound NbS<sub>3</sub>, of collectively carrying electric current above 37°C, the temperature of the human body.<sup>3</sup> Moreover, a significant body of evidence highlights the importance of CDW,<sup>4,5</sup> stripe,<sup>6-8</sup> and other charge- and/or spin-ordered phases in high- $T_c$  and other unconventional superconductors as carrier concentration is varied, e.g. by doping. Some experiments<sup>9</sup> suggest possible interfacial superconductivity or a related phase transition near the boundary between ion-implanted and unimplanted regions of a CDW in NbSe<sub>3</sub>.

Importantly, Aharonov-Bohm (A-B) quantum interference effects, showing oscillations of period  $h/2e$  in CDW conductance vs. magnetic flux, have been reported<sup>10</sup> for TaS<sub>3</sub> rings above 77 K. Similar  $h/2e$  oscillations have been reproduced, as reported in 2012,<sup>11</sup> for at least five TaS<sub>3</sub> rings with circumferences of up to 85  $\mu\text{m}$ . The A-B oscillations are only observed in the CDW (not normal electron) magneto-conductance above the threshold electric field for CDW transport, and the amplitude of the oscillations scales with CDW current. The ring experiments show that, at least for some materials, the CDW condensate exhibits quantum phase coherence over distances of several ten's of microns. There is no classical

sliding CDW explanation for such extraordinary behavior, which manifests Planck's constant at the macroscopic scale. These results thus underscore the need for a fundamental paradigm shift, in which the laws of quantum physics play a crucial role in describing CDW electron transport.

One ring was reported<sup>11</sup> to exhibit telegraph-like temporal switching between high and low CDW current states, the high current state showing substantially larger amplitude  $h/2e$  oscillations than the low current state. This telegraph-like near destruction and reappearance of A-B quantum interference in the CDW ring indicates quasi-periodic loss of quantum coherence, suggesting two types of transport involving either probabilities or probability amplitudes (the former lacking vs. the latter including quantum coherence). Alternatively, the behavior may suggest some form of macroscopically observable "wave-function collapse." Regardless of which interpretation emerges, a deeper understanding of the observed behavior based on the laws of quantum physics could ultimately prove important to condensed matter physics and possibly to the foundations of quantum physics.

Earlier experiments have shown that, in NbSe<sub>3</sub> and TaS<sub>3</sub>, the CDW displaces very little below the threshold electric field for CDW transport. This is evident in NMR experiments<sup>12</sup> showing a 2° CDW phase displacement in NbSe<sub>3</sub>, as compared to the classically predicted 90° displacement just below threshold. Further evidence is provided by dielectric and other ac response (mixing, etc.<sup>13-15</sup>) measurements, which exhibit a flat bias dependence as compared to the classically predicted divergent dielectric response shown in Fig. 1(a). These experiments

reveal that, even just below threshold, each portion of the CDW sits near the bottom of a pinning potential well. This suggests that, for these samples, the measured threshold is substantially smaller than the classical depinning field and likely a Coulomb blockade threshold for charge soliton nucleation.<sup>1,16–18</sup>

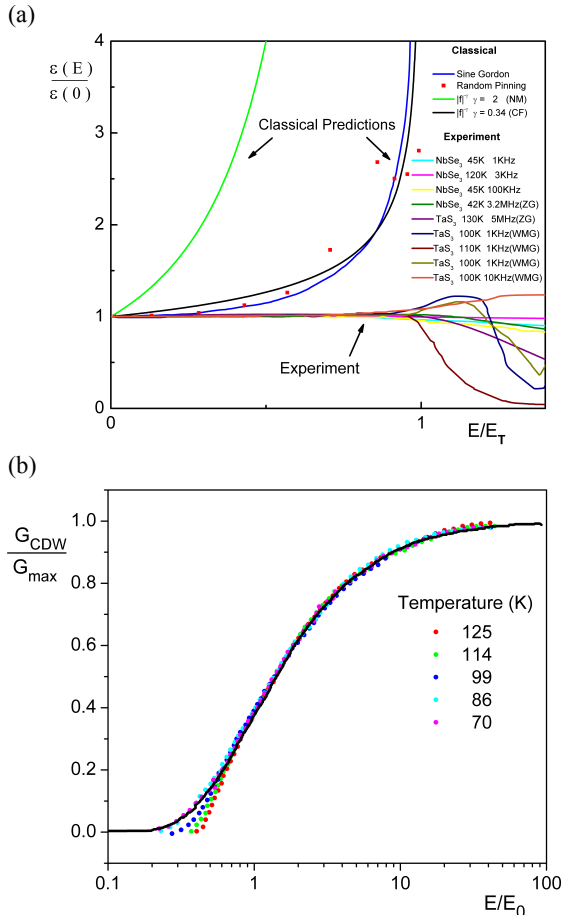


FIG. 1. (a) Bias dependent dielectric response, showing classical predictions vs. experiment. Classical models include classical sine-Gordon, incommensurate harmonic chain (CF),<sup>19</sup> random pinning,<sup>20</sup> renormalization group (NM)<sup>21</sup> models, and where  $f = 1 - E/E_T$ . Some NbSe<sub>3</sub> measurements were carried out in our lab using a bridge circuit, while additional measurements were carried out by ZG<sup>22</sup> and WMG<sup>23</sup> at the indicated temperatures and frequencies. (b) Experimental CDW conductance vs. electric field for NbSe<sub>3</sub> as compared to the Zener tunneling curve  $\exp[-E_0/E]$  (solid line) pointed out by Bardeen.<sup>24</sup> Adapted with permission from ref. <sup>24</sup>, Copyright 1990, American Institute of Physics.

The  $I$ - $V$  characteristic has been found, starting with the early experiments on NbSe<sub>3</sub>,<sup>25</sup> to progress from a rounded Zener tunneling-like characteristic<sup>24</sup> (Fig. 1(b)) to a nearly piecewise linear form in crystals with fewer impurities. This behavior further supports soliton pair creation with a Coulomb blockade threshold.<sup>1,17,18</sup> Soliton pair creation is analogous to Landau-Zener tun-

neling, recently applied to Fermi superfluid gases,<sup>26</sup> Schwinger pair production,<sup>27,28</sup> or creation of superconducting vortex-antivortex pairs.<sup>29</sup> The existing classical models fail to explain the shape of the CDW  $I$ - $V$  curves of NbSe<sub>3</sub> and TaS<sub>3</sub> in a straightforward fashion.<sup>30</sup> Finally, there is no existing classical sliding interpretation for the  $\hbar/2e$  quantum interference effects seen in CDW rings.<sup>10,11</sup> Any viable CDW transport theory of this extraordinary phenomenon must contain Planck's constant, even at the macroscopic level. However, this does not rule out the possibility of using the Schrödinger equation itself as an emergent 'classical' equation, as discussed by Feynman in the context of superconductivity (ref.<sup>31</sup>, vol. III, Ch. 21). This approach, novel for CDWs,<sup>1</sup> of employing the Schrödinger equation to describe classically robust complex order parameters will be discussed in section III. The following section discusses a modified sine-Gordon model, the simplest possible model of a pinned CDW.

## II. PINNED CHARGE DENSITY WAVE AS MASSIVE SCHWINGER MODEL

A CDW has a modulated charge  $\rho(x, t) = \rho_0(x, t) + \rho_1 \cos[2k_F x - \phi(x, t)]$  along the axis of a linear chain compound. Here  $\rho_0(x, t)$  contains background charge and any excess or deficiency of charge  $\propto \partial\phi/\partial x$ . The entire CDW condensate and Peierls gaps, initially at  $\pm k_F$ , can be displaced in momentum space, resulting in a current:  $I_{cdw} \propto \partial\phi/\partial t$ .<sup>32,33</sup> Although a real CDW is pinned by impurities, in some materials it will still transport a current provided the applied field  $E$  exceeds a threshold  $E_T$ . Displacing the CDW by one wavelength (advancing  $\phi$  by  $2\pi$ ) returns the system to its original state (except for charge displaced between contacts) so the pinning energy is periodic in  $\phi$ :  $u_p[1 - \cos\phi]$ . (A quantum version<sup>34</sup> of the Fukuyama-Lee-Rice (FLR) model,<sup>35,36</sup> including disorder, is more accurate but observed voltage oscillations suggest the simple sine-Gordon picture captures much of the physics for high quality crystals.)

Unlike a superconductor, the CDW charge modulation does not couple directly to a uniform electric field or vector potential. However, gradients or kinks in phase carry charges that (1) couple to an externally applied field and (2) generate their own electric fields that lead to electrostatic interactions. These electrostatic interactions between kinks, often neglected in previous theories, are important whether treating the system classically or quantum mechanically. If the CDW phase is initially fixed at zero at the contacts or at  $\pm\infty$ , advancing the phase by  $\phi$  in the middle creates charged kinks that produce an internal field:  $E_\phi = (E^*/2\pi)$ , where  $E^* = 2e/(\epsilon A_{ch})$  is the field created by a  $2\pi$  phase soliton-antisoliton pair and  $A_{ch}$  is the cross-sectional area per chain.

Figure 2 shows the combined effects of the applied field  $E$  and the field  $E^*$  created by a pair of soliton domain walls. The difference in electrostatic energy densities,

$\frac{1}{2}\epsilon(E \pm E^*)^2 - \frac{1}{2}\epsilon E^2$ , with and without the pair is positive when  $E$  is less than the Coulomb blockade threshold field,  $E_T = \frac{1}{2}E^* = en_{ch}/\epsilon$ . Here  $n_{ch} = 1/A_{ch}$  is the number of parallel chains per unit cross-sectional area. The empirically observed relation  $\epsilon E_T \sim en_{ch}$  pointed out by Grüner<sup>37,38</sup> thus emerges naturally from this picture. The simplest classical model predicts<sup>37,38</sup> the classical depinning field  $E_{cl}$  to scale as:  $\epsilon E_{cl} = 4\pi en_{ch}$ , where  $E_{cl} \propto n_i^2$  for weak pinning ( $n_i$  being the impurity concentration). This yields:  $E_T = E_{cl}/4\pi$ , which has the same impurity dependence as  $E_{cl}$  for a fixed temperature. Screening by normal carriers further enhances  $\epsilon$  and reduces the ratio:  $E_T/E_{cl}$ . For fixed  $n_i$ , the temperature dependence of carrier concentration and  $\epsilon$  leads (inversely) to the strong temperature dependence of  $E_T$  seen in some materials. In addition,  $en_{ch}$  is multiplied by the condensate fraction  $\rho_c$  in a more precise description.

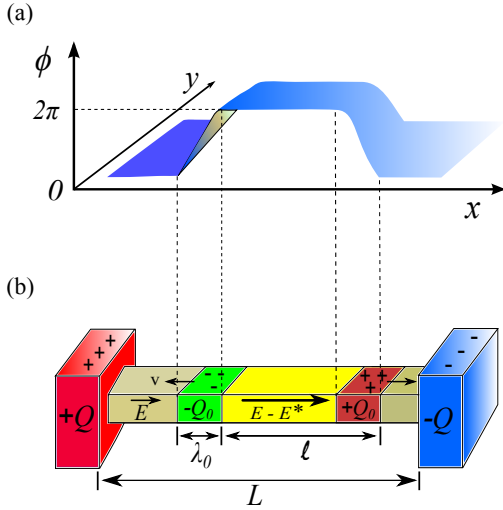


FIG. 2. (a) CDW phase vs. position, showing internal field  $E^*$  produced by a soliton-antisoliton domain wall pair. (b) Model of density wave capacitance showing nucleated domain walls, more realistically depicted as soliton dislocation droplets in section III. The applied field  $E$  partially or completely cancels the internal field  $E^*$ .

Following the quantum field theory literature,  $E$  relates to the ‘vacuum angle’ as  $\theta = 2\pi(E/E^*)$ . For phase displacements  $\phi$  between contacts,  $E$  partially cancels  $E_\phi$ , yielding an electrostatic energy  $u_E(\theta - \phi)^2$ .<sup>1</sup> The potential energy per chain can then be written as<sup>1,18,39</sup>:

$$U[\phi] = \int dx \left\{ 2u_p [1 - \cos \phi(x)] + u_E (\theta - \phi(x))^2 \right\} \quad (1)$$

This is a variant of the bosonic massive Schwinger model, studied as a model of quark confinement<sup>16,40</sup> and first adapted to explain the CDW quantum threshold field by Krive and Rozhavsky.<sup>17</sup> The usual linear coupling  $\propto -\theta\phi$  is contained in the quadratic term, as are electrostatic contributions  $\propto \phi^2$  and  $\theta^2$ . When  $\theta < \pi$ , the system is stable classically and quantum mechanically (Fig. 3). When  $\theta > \pi$ , the  $\phi \sim 2\pi$  state becomes the lowest energy state.

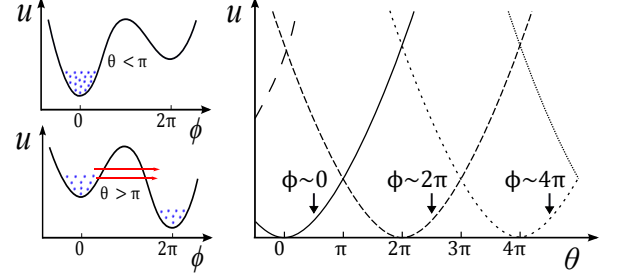


FIG. 3. (Left) Potential energy vs.  $\phi$  for two values of  $\theta$ , with many degrees of freedom illustrated as blue dots. Tunneling can only occur if  $\theta > \pi$  ( $E > E_T$ ), when ‘bubbles’ of the phases  $\phi_k$  for the parallel CDW chains can nucleate by tunneling into the adjacent well. (Right) Potential energy parabolas  $u$  vs.  $\theta$ , in which the phases  $\phi_k \approx \phi$  are sitting in various potential minima,  $\phi \sim 2\pi n$ . The first crossover between parabolic branches occurs at  $\theta = \pi$ .

Thus,  $\theta = \phi$  demarcates the boundary<sup>39</sup> above the system can decay into the lower well. Several quasi-1-D systems appear to be in the sweet spot of interchain interactions - strong enough to avoid being swamped by thermally excited soliton dislocations but not strong enough to remain forever trapped in the higher well. Some NbSe<sub>3</sub> crystals suddenly switch into a higher CDW current-carrying state as the field is increased<sup>41</sup> and show a hysteretic  $I$ - $V$  curve. A natural interpretation is that, as  $\theta$  is increased above  $\pi$ , the system is temporarily trapped in the higher metastable well (Fig. 3) before decaying rapidly into the lower well. Other materials show more than one threshold field.<sup>42,43</sup> The picture here provides a simple interpretation: that the lower threshold field is the Coulomb blockade threshold for soliton nucleation<sup>1,17,18</sup> while the upper threshold is the classical depinning field.

Figure 4(a) shows blue bronze data<sup>43</sup> that, especially at 48 K, exhibits two distinct threshold fields above which the conductance increases. The upper threshold field, presumed to be the classical depinning field  $E_{cl}$ , shows the most dramatic increase in CDW current. The lower threshold field is interpreted as the Coulomb blockade field  $E_{Ts}$  for soliton nucleation. Figure 4(b) shows plots of  $u$  vs.  $\phi$ , illustrating the soliton nucleation ( $\theta \geq \pi$ ) and classical depinning ( $\theta \geq \theta_c$ ) instabilities that arise as  $\theta$  is increased. Figure 4(c) plots  $u$  vs.  $\phi$  when  $\theta = \pi$  for several values of  $u_E/u_p$ . Figure 4(d) shows the resulting phase diagram,<sup>1</sup> which plots  $\theta/\pi = \epsilon E/(\epsilon_1 E_T)$  vs.  $u_E/u_p$  and allows for variations in  $\epsilon$  relative to its threshold value  $\epsilon_1$ . The diagram illustrates the pinned state ( $\theta < \pi, u_E/u_p < 1$ ), a region in which soliton nucleation occurs ( $\pi < \theta < \theta_c$ ), and a classical depinning region ( $\theta > \theta_c$ ).

The flat dielectric and other ac responses<sup>13,15</sup> (Fig. 1) and small phase displacements<sup>12</sup> below threshold in NbSe<sub>3</sub> and TaS<sub>3</sub> suggest  $u_E/u_p \ll 1$  [red arrow in Fig. 4 phase diagram] in these samples. Computed  $\langle \phi \rangle$  below threshold<sup>18</sup> compares favorably to the reported

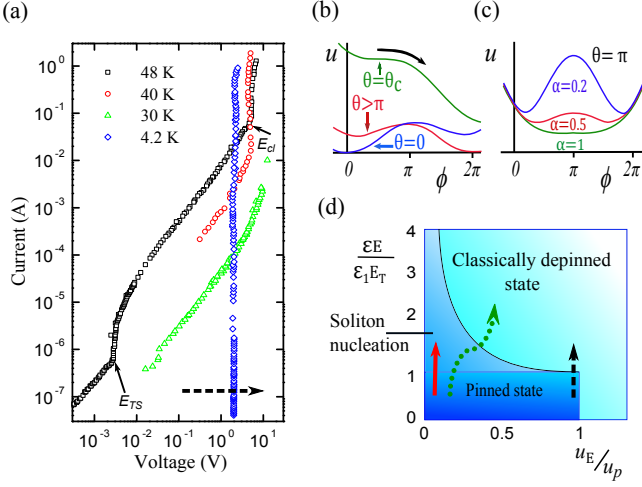


FIG. 4. (a) Blue bronze  $I$ - $V$  curves<sup>43</sup> in which two threshold fields are apparent. (b) Potential energy vs.  $\phi$ , for increasing values of  $\theta$  up to the classical depinning instability  $\theta_c$ . (c)  $u$  vs.  $\phi$  for several ratios  $u_E/u_p$  when  $\theta = \pi$ . (d) Phase diagram<sup>1</sup> showing pinned, soliton nucleation, and classically depinned states. Red arrow ( $u_E/u_p \ll 1$ ) crosses from the pinned state into the soliton nucleation region. The dotted green arrow depicts a system exhibiting both thresholds. Since  $u_E \propto 1/\epsilon$  the path curves to the left (right) if  $\epsilon$  increases (decreases) with field. Dashed black arrows: classical depinning dominates, as suggested by the 4.2-K blue bronze data.

$2^\circ$  value<sup>12</sup> for  $\text{NbSe}_3$  provided  $u_E/u_p \sim 0.015$ .<sup>18</sup> Using  $u_E/u_p = (2\pi E_T)/E_{cl}$ , the 48-K blue bronze data<sup>43</sup> in Fig. 4 suggest a similar value of about 0.01. The increase in  $E_{Ts} (\propto 1/\epsilon)$  with decreasing temperature is readily interpreted as due to a reduction in  $\epsilon$  as the normal carrier concentration decreases. At 4 K, the normal carriers are largely frozen out, resulting in a relatively low  $\epsilon$  and sufficiently high  $u_E/u_p$  for classical depinning to dominate [thick black arrows in Fig. 4]. The following sections discuss CDW dynamics above threshold and the issue of quantum coherence, as revealed by CDW ring<sup>10,11</sup> and other experiments.

### III. TIME-CORRELATED SOLITON TUNNELING MODEL

A basic premise of this paper is that much of the dynamical behavior of CDWs seen in the highest quality crystals of  $\text{NbSe}_3$  and related materials can be understood by extending the simple picture discussed above. These phenomena include narrow-band noise with a fundamental frequency that scales with CDW current and a rich spectrum of harmonics, and complete mode-locking with an external ac source at high drift frequencies (even when much higher than the dielectric relaxation frequency, in contradiction with classical predictions<sup>44</sup>). The key to successfully applying such a simple model is to accept quantum principles, one of which is Gell-Man's to-

talitarian principle:<sup>45</sup> “Everything not forbidden is compulsory.” Applied to CDWs the implication is: *If CDW electrons can tunnel then they must tunnel*. Experiments to date suggest that CDW condensates behave as sticky quantum fluids or deformable quantum solids with dislocations<sup>46</sup> rather than massive classical deformable objects.

Hypotheses addressed in this paper include: 1) low energy phase soliton dislocations of charge  $\pm 2e$  (or, in our view less likely, amplitude solitons of charge  $\pm e$ )<sup>47–51</sup> nucleate above a Coulomb blockade threshold and form droplets resembling fluidic domain walls (soliton liquids), where interchain interactions or Josephson coupling between chains<sup>52</sup> prevent rampant thermal excitations;<sup>30</sup> 2) in the highest quality crystals the nucleation process is best described as coherent Josephson-like tunneling using a modified tunneling matrix element<sup>1</sup> that reflects the Zener probability; 3) in these same materials, the time-evolution of complex order parameters, resembling probability amplitudes, can be described using the Schrödinger equation as an emergent classical equation;<sup>1,31</sup> and 4) both static (e.g. in ring experiments with magnetic flux) and dynamic ( $ac$  response) vector and scalar potentials can couple to and/or modulate the phases of the complex order parameters.

CDWs are often highly anisotropic, where the dielectric response,  $\epsilon_{\parallel x}$ , along the chain direction is much greater than those,  $\epsilon_{\perp y,z}$ , in the perpendicular directions. The degree of anisotropy affects the internal field  $E^*$  generated by a dislocation pair (Fig. 5(a), (b)) and, thus, the Coulomb blockade threshold field:  $E_T = E^*/2$ . One method of modeling this behavior (using COMSOL<sup>53</sup>) is to rescale the variables along the  $x$ -,  $y$ -, and  $z$ -directions by dividing by the relative dielectric constants:  $x' = x/\epsilon_{\parallel}$ ,  $y' = y/\epsilon_{\perp y}$ , and  $z' = z/\epsilon_{\perp z}$ . This is seen starting with the Maxwell equation:  $\nabla \cdot \mathbf{D} = \rho$ , where (using the summation convention):  $D_i = \epsilon_0 \epsilon_{ij} E_j$ . Here  $\epsilon_{ij}$  is the relative dielectric tensor, which is diagonal with elements  $\epsilon_{\parallel} \equiv \epsilon_{xx}$ ,  $\epsilon_{\perp y} \equiv \epsilon_{yy}$ , and  $\epsilon_{\perp z} \equiv \epsilon_{zz}$ , if the axes  $i, j = x, y$ , and  $z$  are along the principal crystallographic directions. Fig. 5(b) illustrates the rescaled COMSOL simulations in 2-D, where the dislocation pair in rescaled coordinates looks like a parallel plate capacitor that produces an internal field  $E^* = 2e/(2\epsilon A_{ch}) = (en_{ch})/\epsilon$ , where  $\epsilon = \epsilon_{\parallel} \epsilon_0$ . This is within a factor of  $\frac{1}{2}$  of the ideal value,  $2en_{ch}/\epsilon$ , for a fully condensed CDW. Figure 5(c) shows the aggregation of many  $2\pi$  dislocations of charge  $2e$  into fluidic soliton droplets that move toward the contacts and allow the bubble of lower energy between them (or ‘true vacuum,’ using the quantum field theory terminology) to grow. Other factors that can affect  $E^*$  and  $E_T$  include gate electrodes in CDW field- and current-effect transistors,<sup>54–59</sup> as well as screening by normal carriers.

The time-correlated soliton tunneling model,<sup>1</sup> which interprets CDW dynamics above threshold, borrows concepts from the theory of time-correlated single electron tunneling.<sup>60,61</sup> The electrostatic energy parabolas of Fig. 3 (also Fig. 6(a)) are similar to the charging en-



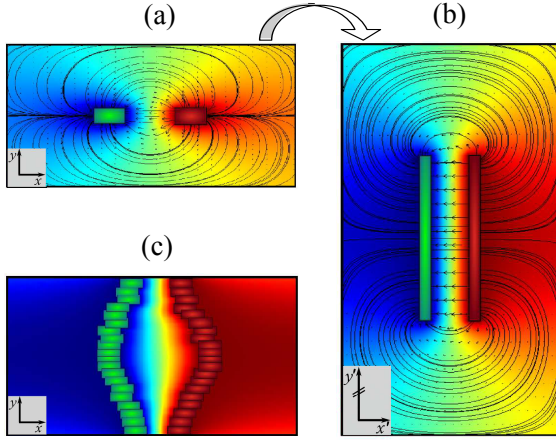


FIG. 5. (a) COMSOL simulation of electrostatic potential (red = positive, blue = negative) and field lines for an electric dipole consisting of dislocations represented as + and - rectangular charge distributions. (b) COMSOL simulation for a similar pair with anisotropic dielectric constants, which resembles a parallel plate capacitor in rescaled coordinates. (c) Aggregation of many dislocations into fluidic domain walls or droplets of soliton liquids, between which the bubble of lower energy or ‘true vacuum’ grows as they are driven toward the contacts by the externally applied field.

ergies of a small-capacitance tunnel junction. According to this model, *coherent voltage oscillations, narrow-band noise, and ac-dc interference effects come from these piecewise parabolic charging energy curves, and not from the shape of the periodic pinning potential.* The large normal carrier concentration in NbSe<sub>3</sub> due to incomplete Peierls gap formation leads to significant screening by normal carriers, which enhances the spatial uniformity of the CDW’s dielectric response. This explains why such highly coherent voltage oscillations, narrow-band noise peaks, and mode locking are often observed<sup>44,62,63</sup> in NbSe<sub>3</sub> crystals, even though the pinning comes from randomly distributed impurities.<sup>34–36</sup> Moreover, the piecewise parabolic curves also explain why the narrow-band noise spectra show such a rich array of harmonics.

The simplest model<sup>1</sup> treats the CDW as a capacitive Coulomb blockade tunnel junction in parallel with a shunt resistor  $R$  (Fig. 6(c)) due to normal uncondensed electrons. To model dynamics, the ‘vacuum angle’ is related to displacement charge  $Q$  between contacts as:  $\theta = 2\pi Q/Q_0$ , where  $Q_0 = 2eN$  and  $N$  is the number of parallel CDW chains. Advancing the phases of all chains by  $2\pi n$  creates multiple pairs of fluidic soliton domain walls that quickly reach the contacts. Similar to a capacitive tunnel junction the voltage is:  $V = (Q - Q_0)/2C = (Q_0/2\pi C)[\theta - 2\pi n]$ , where  $C = \epsilon A/l$ . More generally:  $V = (Q_0/2\pi C)[\theta - \langle\phi\rangle]$ , if  $\langle\phi\rangle \neq 2\pi n$ . The total current is:  $I = I_n + I_{cdw}$ , where  $I_n = (Q_0/2\pi RC)[\theta - \langle\phi\rangle]$  is the normal current and  $I_{cdw} = dQ/dt = (Q_0/2\pi)d\theta/dt$  is the CDW current. (The latter includes capacitive displacement current but is identical to  $(Q_0/2\pi)d\langle\phi\rangle/dt$  when time-averaged.) Defining  $\omega \equiv 2\pi I/Q_0$  and  $\tau \equiv RC$  yields

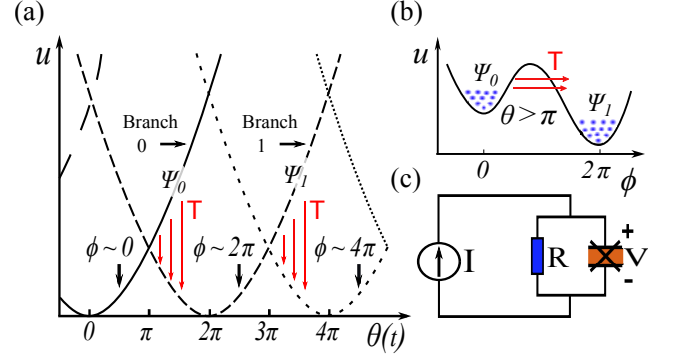


FIG. 6. (a) Potential energy vs.  $\theta$  for  $\phi \sim 2\pi n$ . (b)  $u$  vs.  $\phi$  when  $\theta = 2\pi E/E^* > \pi$  ( $E > E_T$ ) as the phases  $\phi_k(x)$  tunnel coherently into the next well via the tunneling matrix element  $T$ . (c) Time-correlated soliton tunneling model, consisting of a normal shunt resistance  $R$  in parallel with the CDW, represented as a capacitive Coulomb blockade tunnel junction.

the following equation for the time evolution of  $\theta$ :

$$\frac{d\theta}{dt} = \omega - \frac{1}{\tau} [\theta - \langle\phi\rangle]. \quad (2)$$

Since  $\langle\phi\rangle$  advances in a jerky fashion, Eq. (2) contains the elements needed to explain the observed voltage oscillations, narrow-band noise, etc. Within a unified framework it allows for at least three mechanisms by which  $\langle\phi\rangle$  can evolve: (a) coherent Josephson-like tunneling via a matrix element  $T$ , (b) incoherent tunneling or thermal activation of solitons, and (c) classical depinning. Feynman<sup>31</sup> (vol. III, Ch. 21) provides a derivation of coherent Josephson tunneling, where the Schrödinger equation is viewed as a ‘classical’ equation to treat wavefunction-like order parameters coupled by a tunneling matrix element. We have developed<sup>1</sup> a similar method for the CDW to compute  $\langle\phi(t)\rangle$  via the coherent tunneling mechanism (a). It employs the Schrödinger equation:

$$i\hbar \frac{\partial \psi_{0,1}}{\partial t} = U_{0,1} \psi_{0,1} + T \psi_{1,0} \quad (3)$$

to compute the original and emerging probability amplitudes  $\psi_0(t)$  &  $\psi_1(t)$  for the system to be on branches 0 and 1 in Fig. 6(a) (more generally  $\psi_j$  &  $\psi_{j+1}$ ) when coupled by the matrix element  $T$ . The model treats the amplitudes as complex order parameters:

$$\psi_{1,0} = \sqrt{\rho_{0,1}} \exp[i\delta_{0,1}], \quad (4)$$

where  $\delta_{0,1} = N_{0,1}/N$  is the fraction of parallel chains on the respective branch. Advancing the CDW phases  $\phi_k(x)$  of many chains by  $2\pi$  (from one branch to the next in Fig. 6) creates lower energy bubbles bounded by droplets of microscopic  $2\pi$  solitons and antisolitons (somewhat delocalized as quantum solitons<sup>64</sup>) which form the new fluidic macrostate  $\psi_1$ .

The microscopic quantum soliton energy per electron pair,  $\Delta_\varphi$ , can be estimated from the measured Zener field,  $E_0 \sim (\Delta_\varphi^2/\hbar\nu_0 e)$ , typically  $\sim 10$  V/m. Using a phason velocity,  $\nu_0 \sim 3 \times 10^3$  m/s, yields  $\Delta_\varphi \sim 5$   $\mu$ eV, an extremely small value. However, the coupled macrostates have substantial condensation energies due to the many ( $> 10^9$ ) interacting parallel CDW chains.<sup>24,30</sup> The condensed solitons in the emerging macrostate are thus effectively trapped in soliton liquids, preventing thermal excitations except across the much larger Peierls gap. An analogy is provided by Josephson coupling between superimposed macrostates in 2-band superconductors,<sup>65</sup> where thermal excitations only occur across either BCS energy gap regardless of the energy difference between macrostates. One can also view bubbles of the CDW chains escaping out of the metastable well (Fig. 6(b)) as being analogous to superfluid helium atoms quantum mechanically creeping out of a container. If the container rim is, for example,  $d \sim 1$  cm above the liquid surface, then the gravitational barrier per atom is  $mgd \sim 4$  neV, which is small compared to  $kT$  even at 1 mK. Nevertheless, the helium atoms remain trapped in the superfluid, prevented by the condensation energy from thermally hopping out of the container even though they quantum mechanically creep over the rim in a collective fashion.

The driving force  $F$  is the energy difference per unit length after one branch crosses another in Fig. 6(a).<sup>1</sup> Using the analogy to pair production<sup>27</sup> and following Bardeen,<sup>66,67</sup> the tunneling matrix element  $T$  is estimated to be:

$$T(F) = -4F\lambda \exp[-F_0/F], \quad (5)$$

where  $F_0$  ( $\Delta_\varphi^2/(\hbar c_0)$ ) and  $\lambda$  is defined in ref.<sup>1</sup>. Fig. 7(a) compares the simulations with measured voltage oscillations<sup>62</sup> of NbSe<sub>3</sub> for rectangular current pulses. Except for the increasing pulse amplitudes, the same parameters are used for the entire family of theoretical plots (solid lines), which show unprecedented quantitative agreement with experiment. The model correctly captures the progression of non-sinusoidal shapes, ranging from rounded backward sawtooth behavior for the 9.90- $\mu$ A current pulse to more symmetrical oscillations for higher pulse amplitudes. The inset to Fig. 7(a) shows the CDW current ( $I_{cdw} = I - I_n$ ) vs. time corresponding to the 10.89- $\mu$ A pulse. This plot: 1) shows that a large fraction of the CDW current is oscillatory, and 2) captures the ‘flowing,’ rather than abrupt tunneling, aspect of quantum transport. The  $I$ - $V$  and differential resistance curves are computed<sup>1</sup> by averaging over several cycles, with results shown in Figs. 7(b)-(d). A range of behaviors are captured, ranging from rounded Zener-like behavior to more linear  $I$ - $V$  curves and  $dV/dI$  curves with negative dips or wings, as seen in NbSe<sub>3</sub> crystals with fewer impurities.<sup>44</sup> The theoretical plots show outstanding quantitative agreement with experiment in Fig. 7(d).

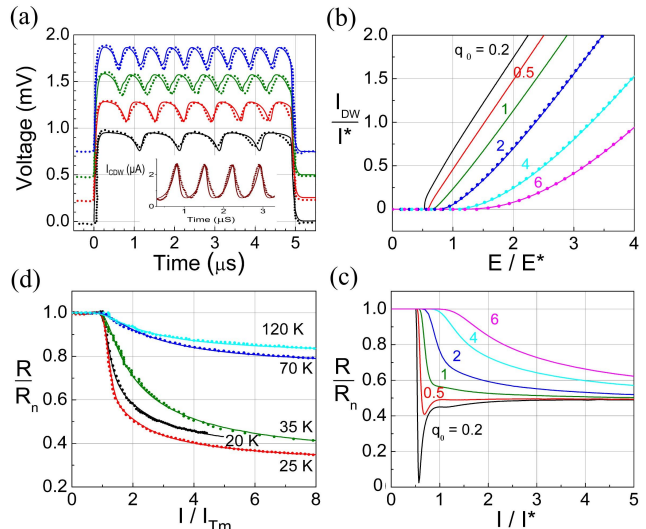


FIG. 7. (a) Theoretical<sup>1</sup> (solid lines) vs. experimental (dotted lines<sup>62</sup>) voltage oscillations (bottom to top, offset by 0, 0.25, 0.5, and 0.75 mV) of an NbSe<sub>3</sub> crystal at 52 K for current pulse amplitudes: 9.90  $\mu$ A (black), 10.89  $\mu$ A (red), 11.49  $\mu$ A (green), & 11.88  $\mu$ A (blue). Inset: CDW current,  $I - I_n$ , vs. time for the 10.89  $\mu$ A pulse. (b) Simulated CDW current vs. field for several  $q_0 = F_0/2eE^*$ . Dotted lines: Bardeen’s modified Zener function.<sup>68</sup> (c) Simulated  $R = dV/dI$  vs. current for several  $q_0$ , where  $R_n$  is the normal resistance below threshold. (d) Theoretical (solid lines) vs. experimental (dotted lines)  $dV/dI$  vs. current for NbSe<sub>3</sub> (see<sup>1</sup> for parameters).

#### IV. COUPLING OF ORDER PARAMETER PHASES TO VECTOR AND SCALAR POTENTIALS

The simulations of dc transport and rectangular current pulses, discussed above, fix the phase difference  $\delta \equiv \delta_{j+1} - \delta_j$  at  $\pi/2$  in Eq. (3),<sup>1</sup> which yields the maximum current in the Josephson current-phase relation. This section discusses coupling of static (magnetic field) and dynamic ( $ac$  electric field) vector and scalar potentials to the phases  $\delta_j$  in order to: a) interpret the  $h/2e$  quantum interference effects in CDW rings;<sup>10,11</sup> b) better understand mixing and other  $ac$  response experiments,<sup>13–15</sup> previously interpreted using photon-assisted tunneling (PAT) theory;<sup>69</sup> and c) interpret new large amplitude  $ac$  experiments presented here. The ability to vary both magnitudes and phases of the macrostate amplitudes could eventually set the stage for development of future quantum computing devices, while better understanding of the ring experiments could enable new types of magnetic sensors.

In the CDW ring experiments<sup>10,11</sup> a static magnetic vector potential couples to the phases  $\delta_j$  and leads to quantum interference between the amplitudes traversing the two branches of the ring (nucleated quantum solitons interfering with themselves). This can be visualized in terms of an extra phase shift  $\chi$  affecting the tunneling matrix elements of a two-domain model:

$$T_{a,b} \rightarrow T \exp [\pm i\chi/2], \quad (6)$$

one domain for each path,  $a$  or  $b$ , along the ring. Here:

$$\chi = \frac{q}{\hbar} \oint \mathbf{A} \cdot d\mathbf{r} = 2\pi [\Phi/\Phi_0], \quad (7)$$

where  $\Phi_0 = h/q$  and  $q$  is either  $e$  or  $2e$ . Summing the amplitudes then yields a modulation proportional to  $|2T \cos[\Phi/\Phi_0]|$ . This simple two-domain picture gives the correct period  $h/2e$  for the A-B oscillations provided we take  $q = 2e$ . However, it is an oversimplification compared to the reported  $\sim 10\%$  modulation and rather disordered behavior in the A-B oscillations in the actual CDW rings<sup>10,11</sup>, suggesting the need to include many CDW domains with some degree of disorder. Moreover,  $ac$  response experiments, discussed below, suggest a rather short tunneling distance. This further indicates the need to incorporate multiple domains, which can be modeled as a network of many tunnel junctions in series.

The phases  $\delta_i(t)$  of the macrostate order parameters in Eq. (4) can be modulated by an oscillatory field that temporally evolves the scalar and/or vector potentials. The theory of photon-assisted tunneling (PAT)<sup>69</sup> enables predictions of tunnel junction response to combined  $dc$  and  $ac$  signals based on its  $dc$  current-voltage ( $I$ - $V$ ) characteristic. Oscillatory voltages modulate the relative energies and phases of wavefunctions on opposite sides of the tunnel junction. This generates various combinations of Bessel functions in the predicted responses, which reduce to finite differences of the  $I$ - $V$  curves in the small-signal limit. A modification of PAT theory was previously adapted to interpret mixing and other CDW  $ac$  response experiments<sup>13-15</sup> on TaS<sub>3</sub> and NbSe<sub>3</sub>. These experiments show good agreement with PAT theory for small-amplitude signals.<sup>13-15</sup> Mixing experiments apply a signal of the form:

$$V(t) = V_{dc} + V_1 \cos \omega_1 t + V_2 \cos \omega_2 t \quad (8)$$

and measure an induced response (e.g. with a lock-in amplifier):  $\delta I(t) = \delta I_0 \cos[\omega_0 t + \varphi]$ . The difference frequency is:  $\omega_0 = |\omega_2 - \omega_1|$  for direct mixing and  $\omega_0 = |\omega_2 - 2\omega_1|$  for harmonic mixing. At low frequencies and amplitudes, the harmonic mixing response vs. bias voltage  $V_{dc}$  is proportional to the third derivative of the  $dc$   $I$ - $V$  curve:

$$\delta I_0(V_{dc}) = \frac{1}{8} V_1^2 V_2 \left[ \frac{d^3 I_{dc}}{dV^3} \right]_{V=V_{dc}}. \quad (9)$$

At finite frequencies, the third derivative gets replaced by a third finite difference<sup>15</sup> with a step size proportional to frequency but has a similar, albeit broadened, bias dependence. The harmonic mixing response at zero  $dc$  bias voltage becomes significant for frequencies  $\omega_0/2\pi$

of about 1 MHz and greater, and is found to be bias-independent below threshold.<sup>15</sup>

Rather different behavior emerges when the  $dc$  bias voltage  $V_{dc}$  in Eq. (8) is replaced by a large amplitude  $ac$  ‘bias’ voltage,

$$V_{dc} \rightarrow V_{dc} \cos \omega t, \quad (10)$$

and the harmonic mixing response  $\delta I_0$  is plotted vs.  $V_{ac}$ . When  $\omega$  is small, since harmonic mixing is an even function of  $dc$  bias,  $\delta I_0(V_{ac})$  is just the time-averaged response vs. bias voltage  $\langle \delta I_0(V_{bias}(t)) \rangle$ , which resembles a washed out third derivative. When  $\omega/2\pi$  reaches about 50 kHz or higher, however,  $\delta I_0(V_{ac})$  resembles  $\delta I_0(V_{dc} - V_T)$  with an apparent threshold voltage collapsed to the origin<sup>15</sup>, possibly because of capacitive coupling due to the extremely high CDW dielectric response.

The most interesting behavior is expected to occur when  $\omega$  is at megahertz frequencies and higher. In the absence of coupling  $T$ , a state of modulated energy  $E_{0,1}$  corresponding to branch 0 or 1 in Fig. 6 would evolve as:

$$\psi_{0,1}(t) = \psi_{0,1}(0) \exp \left[ -(i/\hbar) \int_0^t dt' E_{0,1}(t') \right]. \quad (11)$$

Taking the charge to be  $2e$ , the voltage  $V_\ell(t) = V_\ell \cos \omega t$  across a small domain of length  $\ell$  modulates the energy  $E_1(t)$  of state 1 relative to  $E_0$ , as:  $\Delta E(t) = 2eV_\ell \cos \omega t$ . State  $\psi_1$  then evolves relative to  $\psi_0$  as:

$$\begin{aligned} \psi_1(t) &= \psi_1(0) \exp[-iz \sin \omega t] \\ &= \psi_0(0) \sum_{n=-\infty}^{\infty} J_n(z) \exp[-in\omega t], \end{aligned} \quad (12)$$

where  $J_n(z)$  are Bessel functions and  $z \equiv (2eV_\ell)/\hbar\omega$ . This effectively splits up the  $\psi_1$  amplitude into many,

$$\psi'_n = J_n(z) \psi_1, \quad (13)$$

of virtual energy  $E_n = n\hbar\omega$ . ‘Turning on’ the tunneling matrix element  $T$  enables it to couple states  $\psi_0$  &  $\psi'_n$  of equal energy, any negative energy difference being balanced by the soliton pair energy.

Equation (13) thus captures the essence of photon-assisted tunneling, where an initially occupied state can tunnel into an unoccupied state of equal virtual energy. Recalling the relation between harmonic mixing and  $dc$  bias voltage (Eq. (9) and finite difference forms<sup>15</sup>), following PAT theory,<sup>69,70</sup> and noting that  $J_{-n}(x) = (-1)^n J_n(x)$ , the harmonic mixing response vs. total voltage amplitude  $V_{ac}$  between contacts would then be expected to be given by:

$$\begin{aligned} \delta I_0(V_{ac}) &= J_0^2 \left( \frac{V_{ac}}{\alpha\omega} \right) \delta I_0(V_{dc} = 0) + \\ &+ 2 \sum_{n=1}^{\infty} J_n^2 \left( \frac{V_{ac}}{\alpha\omega} \right) \delta I_0(V_0 = n\alpha\omega) \end{aligned} \quad (14)$$

where  $V_0 = V_{dc} - V_T$  due to the collapsed effective  $I$ - $V$  curve<sup>15</sup> at finite frequencies. The amplitudes and frequencies,  $V_1$ ,  $V_2$ ,  $\omega_1$ , and  $\omega_2$ , of the signals inducing the harmonic mixing response are fixed in these experiments.

The scaling parameter  $\alpha$  in Eq. (14) depends on the distance  $L$  between contacts and an effective scaling length  $\ell$ , which relates the energy acquired by a particle of charge  $e^*$  in an electric field  $E$  to a quantum of energy  $\hbar\omega$ :  $e^*V_\ell = e^*El \leftrightarrow \hbar\omega$ . Previously,<sup>71</sup> the effective charge was assumed to be a reduced by the Fröhlich mass ratio,  $e^* \sim [m/M_F]e \sim 10^{-3}e$ , which yielded values of  $\ell$  in the range 1.6-22  $\mu\text{m}$ .<sup>71</sup> Motivated by the recent CDW A-B ring experiments,<sup>10,11</sup> here we take the effective charge to be:  $e^* = 2e$ , which reduces the estimated values of  $\ell$  into the nanometer range. In general, the nature of Zener-like tunneling through a tilted soliton gap may yield some degree of frequency- and/or field-dependence of  $\ell$ . Using  $V_{ac} = (L/\ell)V_\ell$ , one obtains the following scaling parameter:

$$\alpha = \frac{L}{\ell} \frac{\hbar}{2e}. \quad (15)$$

Due to the properties of Bessel functions, the  $J_0^2(V_{ac}/\alpha\omega)$  term in Eq. (14) should initially dominate for small amplitudes,  $V_{ac}$ , while the remaining terms may become significant for larger  $V_{ac}$ . Defining  $\delta I_m \equiv \delta I_0(V_{ac} = 0)$ , restricting  $A_n(\omega) \equiv 2\delta I_0(n\alpha\omega)/\delta I_m$  to be real, and keeping a finite number,  $N$ , of terms, the normalized theoretical harmonic mixing response can be approximated as:

$$\frac{\delta I_o}{\delta I_m} \cong J_0^2\left(\frac{V_{ac}}{\alpha\omega}\right) + \sum_{n=1}^N A_n(\omega) J_n^2\left(\frac{V_{ac}}{\alpha\omega}\right). \quad (16)$$

Figures 8 and 9 show plots of normalized harmonic mixing responses  $|\delta I_0|/|\delta I_m|$  vs.  $ac$  bias amplitude  $V_{ac}$  for single crystals of TaS<sub>3</sub> and NbSe<sub>3</sub>, as compared to Eq. (16). Figure 8(a) shows measured harmonic mixing responses of a TaS<sub>3</sub> crystal ( $L = 0.1$  mm) with a 5 mV threshold voltage at 180 K, for three different  $ac$  bias frequencies  $\omega$ . Figure 8(b) shows theoretical plots using Eq. (16) and the parameters in Table I. For this sample the effective scaling distance  $\ell$ , estimated using Eq. (15) from the parameter  $\alpha$ , is found to be in the range 8-15 nm, or several CDW wavelengths. The extremely small soliton energy gap per electron pair enables this distance to be longer than one would normally encounter in an ordinary tunnel junction.

TABLE I. Eq. (16) parameters used for the Fig. 8(b) theoretical plots.

$\omega/2\pi$ (MHz)	$\alpha$ (V·s)	$A_1$	$A_2$	$A_3$	$A_4$
40	$5.5 \times 10^{-12}$	1.75	0.25	0.42	-1.00
80	$4.2 \times 10^{-12}$	1.80	1.40	0.50	-0.60
160	$3.2 \times 10^{-12}$	2.00	0.70	1.57	1.44

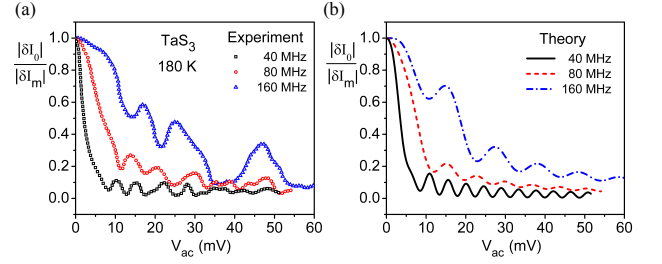


FIG. 8. (a) Normalized magnitude of harmonic mixing response ( $\omega_1/2\pi = 5$  MHz,  $\omega_2/2\pi = 14$  MHz,  $\omega_0/2\pi = 4$  MHz) of a 0.1-mm long TaS<sub>3</sub> crystal, with a  $dc$  threshold  $V_T = 5$  mV, vs.  $ac$  bias amplitude  $V_{ac}$  at three different frequencies  $\omega/2\pi$  at 180 K. (b) Theoretical plots using Eq. (16) and the parameters shown in Table I.

Figure 9 shows measured harmonic mixing responses of an NbSe<sub>3</sub> crystal ( $L = 5$  mm) at 120 K, for several  $ac$  bias frequencies  $\omega$ . Figure 9(a) shows experimental plots, while Fig. 9(b) shows theoretical plots using Eq. (16) and the parameters in Table II. Figures 9(c) and 9(d) directly compare experiment with theory for  $ac$  bias frequencies of 4 MHz and 8 MHz. For this sample the effective scaling length  $\ell$ , estimated using Eq. (15) from the scaling parameter  $\alpha$ , is found to be 1.5 nm, or slightly greater than one CDW wavelength. Here, the shorter length  $\ell$  may reflect a reduced effective mean free path length for the quantum solitons due to the incomplete Peierls gap and large number of uncondensed normal carriers in NbSe<sub>3</sub>. It will be interesting, in future studies, to determine whether the CDW wavelength represents a lower bound on  $\ell$ .

TABLE II. Eq. (16) parameters used for the Fig. 9 theoretical plots.

$\alpha = 1.1 \times 10^{-9}$ (V·s)	$A_1$	$A_2$	$A_3$	$A_4$
4 MHz	0.40	0.65	0.15	0.55
5 MHz	0.45	0.70	-0.30	0.10
6 MHz	0.30	1.00	-1.40	1.90
7 MHz	0.20	1.10	-2.00	3.50
8 MHz	0.20	1.40	-1.65	0.70
10 MHz	0.15	1.90	-1.90	-1.95
15 MHz	0.01	3.00	3.00	1.00

The experiments reported here, as well as earlier mixing experiments at temperatures sometimes exceeding 200 K,<sup>13-15</sup> are consistent with the idea that oscillatory electric potentials modulate the phases of classically robust order parameters resembling macroscopic wavefunctions. Moreover, the experimental results are consistent with those of the CDW ring experiments,<sup>10,11</sup> which demonstrate a significant degree of CDW quantum coherence. Collectively, the experiments support the hypothesis that either a vector or scalar potential couples to order parameter phases of CDW soliton condensates, and in some cases can lead to quantum interference. Fur-



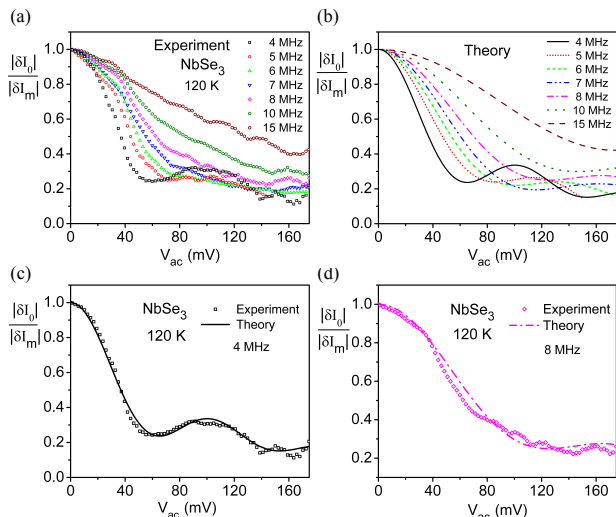


FIG. 9. (a) Normalized magnitude of harmonic mixing response ( $\omega_1/2\pi = 1$  MHz,  $\omega_2/2\pi = 2.8$  MHz,  $\omega_0/2\pi = 800$  kHz) of an NbSe<sub>3</sub> crystal ( $L = 5$  mm), vs.  $ac$  bias amplitude  $V_{ac}$  at several frequencies  $\omega/2\pi$  at 120 K. (b) Theoretical plots using Eq. (16) and the parameters shown in Table II. (c) and (d) Direct comparisons between theory and experiment for frequencies  $\omega/2\pi$  of 4 MHz and 8 MHz.

ther experimental and theoretical studies are warranted to enable the eventual development of a microscopic description of CDW transport.

## V. DISCUSSION AND CONCLUSION

CDW transport is one of the few known cases of correlated transport of macroscopic numbers of electrons - the only known example of large-scale collective electron transport at human body temperatures.<sup>3</sup> This paper is highly transformative in that it challenges the classical sliding CDW paradigm that has dominated the field for over thirty years. Nevertheless, the quantum ideas discussed here can hardly be regarded as speculative. The evidence supporting quantum theory is so enormous, it can be considered a proven fact that electrons and all other known particles behave quantum mechanically. In 2000, the 100-year anniversary of Planck's black-body radiation paper,<sup>72</sup> Kleppner and Jackiw<sup>73</sup> pointed out that: "Quantum theory is the most precisely tested and most successful theory in the history of science." Since then, aspects of quantum theory (the Pauli principle<sup>74</sup>) have been confirmed to within an accuracy of  $6 \times 10^{-29}$ .

The classical behavior one observes on the macroscopic

scale depends on the system and emerges from the behavior of large numbers of entangled quantum particles exhibiting wave-particle duality. The Schrödinger equation can be regarded as the 'classical' equation for superconducting condensates coupled through a thin insulator by Josephson tunneling (vol. III, Ch. 21 of<sup>31</sup>). Similarly, the time-correlated soliton tunneling model discussed here treats the Schrödinger equation as an emergent classical equation describing Josephson-coupled fluidic CDW macrostates. The simulations yield unprecedented quantitative agreement with coherent voltage oscillations and  $I$ - $V$  characteristics of NbSe<sub>3</sub> and also provide a natural interpretation for the quantum interference seen in the CDW ring experiments<sup>10,11</sup> and more complex interesting behavior seen in CDW harmonic mixing response.

Any further progress in understanding of CDW transport will require the scientific community to accept the fact that the CDW electron-phonon condensate behaves according to laws of quantum physics - the same quantum principles that govern every other system of particles in the universe. It is not necessarily true, *a priori*, that quantum principles are consistent with the current dogma - that CDW electrons classically "slide" according to Aristotle's linear velocity-force relation. Addressing the quantum behavior of CDWs, perhaps culminating in a microscopic theory of CDW transport and dynamics, would have enormous impact on this important branch of condensed matter physics. Additional areas of broad impact potentially include the boundary between CDWs and superconductivity, correlated electron-ion transport in biological systems, tunneling and 'false vacuum decay' in quantum cosmology, a formally similar  $\theta = \pi$  instability for spontaneous  $CP$  violation,<sup>75</sup> and a deeper understanding of quantum theory and the emergence of classical reality at the macroscopic scale. Observation of quantum effects in NbS<sub>3</sub>, which undergoes a Peierls transition well above room temperature,<sup>3</sup> would potentially lead to new devices such as magnetic sensors operating at room temperature. Understanding of the quantum behavior of solitons could lead to topologically robust (against decoherence) forms of quantum information processing, which would have major technological significance.

## ACKNOWLEDGMENTS

The authors gratefully acknowledge supported by the State of Texas through the Texas Center for Superconductivity at the University of Houston, the Robert A. Welch Foundation (E-1297), and the Air Force Office of Scientific Research.

\* jhmiller@uh.edu

† aiwijesinghe@yahoo.com

<sup>1</sup> J. H. Miller, Jr., A. I. Wijesinghe, Z. Tang, and A. M. Gu-

loy, Physical Review Letters **108**, 036404 (2012).

<sup>2</sup> P. Monceau, Advances in Physics **61**, 325 (2012).

<sup>3</sup> S. G. Zybtsev, V. Y. Pokrovskii, V. F. Nasretdinova, and

- S. V. Zaitsev-Zotov, *Applied Physics Letters* **94**, 152112 (2009).
- <sup>4</sup> G. Ghiringhelli, et al., *Science* **337**, 821 (2012).
  - <sup>5</sup> J. Chang, et al., *Nature Physics* **8**, 871 (2012).
  - <sup>6</sup> J. M. Tranquada, B. J. Sternlieb, J. D. Axe, Y. Nakamura, and S. Uchida, *Nature* **375**, 561 (1995).
  - <sup>7</sup> V. J. Emery, S. A. Kivelson, and J. M. Tranquada, *Proceedings of the National Academy of Sciences* **96**, 8814 (1999).
  - <sup>8</sup> E. Berg, E. Fradkin, S. A. Kivelson, and J. M. Tranquada, *New Journal of Physics* **11**, 115004 (2009).
  - <sup>9</sup> J. P. McCarten, T. C. Jones, X. Wu, J. H. Miller, Jr., I. Pirtle, X. Xu, J. R. Claycomb, J.-R. Liu, and W.-K. Chu, *Journal de Physique IV France* **9**, 129 (1999).
  - <sup>10</sup> M. Tsubota, K. Inagaki, and S. Tanda, *Physica B: Condensed Matter* **404**, 416 (2009).
  - <sup>11</sup> M. Tsubota, K. Inagaki, T. Matsuura, and S. Tanda, *EPL (Europhysics Letters)* **97**, 57011 (2012).
  - <sup>12</sup> J. H. Ross, Z. Wang, and C. P. Slichter, *Physical Review Letters* **56**, 663 (1986).
  - <sup>13</sup> J. H. Miller, Jr., Dissertation, University of Illinois at Urbana-Champaign, 1985.
  - <sup>14</sup> J. H. Miller, J. Richard, J. R. Tucker, and J. Bardeen, *Physical Review Letters* **51**, 1592 (1983).
  - <sup>15</sup> J. H. Miller, R. E. Thorne, W. G. Lyons, J. R. Tucker, and J. Bardeen, *Physical Review B* **31**, 5229 (1985).
  - <sup>16</sup> S. Coleman, *Annals of Physics* **101**, 239 (1976).
  - <sup>17</sup> I. V. Krive and A. S. Rozhavsky, *Solid State Communications* **55**, 691 (1985).
  - <sup>18</sup> J. H. Miller, C. Ordóñez and E. Prodan, *Physical Review Letters* **84**, 1555 (2000).
  - <sup>19</sup> S. N. Coppersmith and D. S. Fisher, *Physical Review A* **38**, 6338 (1988).
  - <sup>20</sup> P. B. Littlewood, *Physical Review B* **33**, 6694 (1986).
  - <sup>21</sup> O. Narayan and A. A. Middleton, *Physical Review B* **49**, 244 (1994).
  - <sup>22</sup> A. Zettl and G. Grüner, *Physical Review B* **29**, 755 (1984).
  - <sup>23</sup> W.-y. Wu, L. Mihaly, and G. Grüner, *Solid State Communications* **55**, 663 (1985).
  - <sup>24</sup> J. Bardeen, *Physics Today* **43**, 25 (1990).
  - <sup>25</sup> P. Monceau, N. P. Ong, A. M. Portis, A. Meerschaut, and J. Rouxel, *Physical Review Letters* **37**, 602 (1976).
  - <sup>26</sup> W.-Y. Wang, W.-S. Duan, J.-A. Sun, and Y. Yang, *Physica B: Condensed Matter* **407**, 3876 (2012).
  - <sup>27</sup> T. D. Cohen and D. A. McGady, *Physical Review D* **78**, 036008 (2008).
  - <sup>28</sup> Y. Kluger, J. M. Eisenberg, B. Svetitsky, F. Cooper, and E. Mottola, *Physical Review Letters* **67**, 2427 (1991).
  - <sup>29</sup> J. H. Miller, Jr. and A. I. Wijesinghe, in *arXiv:1110.2537v1 [cond-mat.supr-con]* (Los Alamos National Laboratory, Los Alamos, New Mexico, USA, 2011), Vol. <http://arxiv.org/abs/1110.2537>, p. 1.
  - <sup>30</sup> J. Bardeen, *Physical Review B* **39**, 3528 (1989).
  - <sup>31</sup> R. P. Feynman, R. B. Leighton, and M. Sands, *The Feynman Lectures on Physics* (Addison-Wesley, Reading, Massachusetts, 1965).
  - <sup>32</sup> D. Allender, J. W. Bray, and J. Bardeen, *Physical Review B* **9**, 119 (1974).
  - <sup>33</sup> H. Fröhlich, *Proceedings of the Royal Society of London. Series A. Mathematical and Physical Sciences* **223**, 296 (1954).
  - <sup>34</sup> I. V. Krive and A. S. Rozhavsky, *Physics Letters A* **132**, 363 (1988).
  - <sup>35</sup> H. Fukuyama and P. A. Lee, *Physical Review B* **17**, 535 (1978).
  - <sup>36</sup> P. A. Lee and T. M. Rice, *Physical Review B* **19**, 3970 (1979).
  - <sup>37</sup> G. Grüner, *Reviews of Modern Physics* **60**, 1129 (1988).
  - <sup>38</sup> W.-y. Wu, A. Jánossy, and G. Grüner, *Solid State Communications* **49**, 1013 (1984).
  - <sup>39</sup> J. H. Miller, Jr, *Journal of Physics: Conference Series* **273**, 012007 (2011).
  - <sup>40</sup> S. Coleman, R. Jackiw, and L. Susskind, *Annals of Physics* **93**, 267 (1975).
  - <sup>41</sup> A. Zettl and G. Grüner, *Physical Review B* **26**, 2298 (1982).
  - <sup>42</sup> M. E. Itkis, F. Y. Nad, and P. Monceau, *Journal of Physics: Condensed Matter* **2**, 8327 (1990).
  - <sup>43</sup> G. Mihály and P. Beauchêne, *Solid State Communications* **63**, 911 (1987).
  - <sup>44</sup> R. E. Thorne, J. R. Tucker, and J. Bardeen, *Physical Review Letters* **58**, 828 (1987).
  - <sup>45</sup> G. Johnson, *Strange Beauty: Murray Gell-Mann and the Revolution in Twentieth Century Physics* (Vintage Books, Random House, New York; Toronto, 1999).
  - <sup>46</sup> P. W. Anderson, *Basic Notions of Condensed Matter Physics* (Benjamin / Cummings Publishing Co., Menlo Park, California, 1984).
  - <sup>47</sup> S. Brazovskii, *Journal of Superconductivity and Novel Magnetism* **20**, 489 (2007).
  - <sup>48</sup> S. Brazovskii, *Solid State Sciences* **10**, 1786 (2008).
  - <sup>49</sup> S. Brazovskii, *Physica B: Condensed Matter* **404**, 482 (2009).
  - <sup>50</sup> S. Brazovskii, C. Brun, Z.-Z. Wang, and P. Monceau, *Physical Review Letters* **108**, 096801 (2012).
  - <sup>51</sup> N. Kirova, A. Rojo Bravo, and S. Brazovskii, *Physica B: Condensed Matter* **404**, 565 (2009).
  - <sup>52</sup> Y. I. Latyshev, in *ECRYS-2011, International School and Workshop on Electronic Crystals*, Cargse, Corsica, France, 2011).
  - <sup>53</sup> COMSOL Multiphysics (Stockholm, Sweden; Palo Alto, California)
  - <sup>54</sup> T. L. Adelman, S. V. Zaitsev-Zotov, and R. E. Thorne, *Physical Review Letters* **74**, 5264 (1995).
  - <sup>55</sup> J. H. Miller, Jr, G. Cardenas, A. Garcia-Perez, W. More, and A. W. Beckwith, *Journal of Physics A: Mathematical and General* **36**, 9209 (2003).
  - <sup>56</sup> A. Ayari and P. Monceau, *Physical Review B* **66**, 235119 (2002).
  - <sup>57</sup> C. Li, D. Yin, D. Li, Z. Tang, J. Wang, R. Xiong, J. Shi, and D. Tian, *Solid State Communications* **140**, 369 (2006).
  - <sup>58</sup> N. Marković, M. A. H. Dohmen, and H. S. J. van der Zant, *Physical Review Letters* **84**, 534 (2000).
  - <sup>59</sup> S. Yue, M. Tian, and Y. Zhang, *Physical Review B* **64**, 113102 (2001).
  - <sup>60</sup> D. V. Averin and K. K. Likharev, *Journal of Low Temperature Physics* **62**, 345 (1986).
  - <sup>61</sup> D. V. Averin and K. K. Likharev, in *Mesoscopic Phenomena in Solids*, edited by B. L. Altshuler, P. A. Lee and R. A. Webb (Elsevier, Amsterdam, 1991), p. 173.
  - <sup>62</sup> T. C. Jones, X. Wu, C. R. Simpson, J. A. Clayhold, and J. P. McCarten, *Physical Review B* **61**, 10066 (2000).
  - <sup>63</sup> R. E. Thorne, J. S. Hubacek, W. G. Lyons, J. W. Lyding, and J. R. Tucker, *Physical Review B* **37**, 10055 (1988).
  - <sup>64</sup> A. Maiti and J. H. Miller, *Physical Review B* **43**, 12205 (1991).
  - <sup>65</sup> A. J. Leggett, *Progress of Theoretical Physics* **36**, 901 (1966).

- <sup>66</sup> J. Bardeen, Physical Review Letters **6**, 57 (1961).
- <sup>67</sup> C. B. Duke, Tunneling in Solids (Academic Press, New York, 1969).
- <sup>68</sup> J. Bardeen, Physical Review Letters **45**, 1978 (1980).
- <sup>69</sup> J. R. Tucker and M. J. Feldman, Reviews of Modern Physics **57**, 1055 (1985).
- <sup>70</sup> P. K. Tien and J. P. Gordon, Physical Review **129**, 647 (1963).
- <sup>71</sup> R. E. Thorne, J. H. Miller, W. G. Lyons, J. W. Lyding, and J. R. Tucker, Physical Review Letters **55**, 1006 (1985).
- <sup>72</sup> M. Planck, Verhandlungen der Deutschen Physikalischen Gesellschaft **2**, 237 (1900).
- <sup>73</sup> D. Kleppner and R. Jackiw, Science **289**, 893 (2000).
- <sup>74</sup> J. Marton, et al., AIP Conference Proceedings **1327**, 423 (2011).
- <sup>75</sup> D. Boer and J. K. Boomsma, Physical Review D **78**, 054027 (2008).